Corrosion Analysis of Offshore Oil and Gas Pipelines in Africa: Nonlinear Finite Element Assessment of Burst Pressure

Adewunmi Odedina*, Morrison Inegiyemiema, King Nyeche Wugha

Department of Marine and Offshore Engineering, Faculty of Engineering, Rivers State University, Nkpolu-Oroworukwo, Port Harcourt, Rivers State, Nigeria

*** Corresponding author**

DOI: https://doi.org/10.51584/IJRIAS.2026.11090119

Received: 30 September 2026; Accepted: 05 October 2026; Published: 20 October 2026

ABSTRACT

Corrosion-induced metal loss reduces the burst capacity of ageing offshore pipelines, yet its effect on pipelines in African offshore fields remains poorly quantified. This study presents a nonlinear finite element analysis (FEA) of an API 5L X70 steel pipeline (outside diameter 600 mm, wall thickness 30 mm) containing a rectangular corrosion defect (depth-to-wall-thickness ratio 0.667, length-to-width ratio 2) under internal pressure, using design data from the ultra-deepwater Medgaz pipeline as a representative case. A quarter-symmetry three-dimensional model was developed in ANSYS Workbench with multilinear isotropic hardening and large-strain, large-displacement formulations. Internal pressure was increased incrementally from 10 to 45 MPa, and failure initiation was defined as the von Mises stress along a radial path through the defect reaching the ultimate tensile strength of 535 MPa. This local criterion gave a failure pressure of 30 MPa, at which the maximum von Mises stress was 548.02 MPa. Stress, strain and deformation concentrated at the centre of the defect, with hoop stress the dominant component. The FEA pressure was 28–36% lower than the failure pressures given by DNV-RP-F101 (46.55 MPa), PCORRC, ASME B31G and modified B31G (41.9–46.6 MPa), so the criterion gives a conservative estimate for this deep defect. A parametric study showed that peak hoop stress at the failure pressure is not by itself a measure of remaining strength: it fell as the defect became longer and wider, whereas the code-based failure pressure decreases with defect length. The results provide a conservative numerical basis for defect screening and fitness-for-service assessment in the integrity management of offshore pipelines in African operating environments.

Keywords: Corrosion; offshore pipeline; finite element analysis; burst pressure; DNV-RP-F101

INTRODUCTION

Offshore oil and gas pipelines carry hydrocarbons from offshore fields to onshore processing and distribution terminals and are central to energy supply and government revenue in producing countries (Deloitte, 2023; International Energy Agency, 2024; Zhu et al., 2024). Africa holds large offshore reserves, with major production in Nigeria, Angola, Ghana, Egypt, Libya, Algeria, Mozambique and Tanzania, and the growth of deepwater and ultra-deepwater development has increased investment in pipeline systems (Fyrileiy et al., 2013; Monde, 2024).

These pipelines operate under continuous seawater exposure, high pressure, thermal variation, currents, wave loading, seabed movement and corrosive fluids (Chen & Guedes Soares, 2023; Chohan et al., 2024; Yan et al., 2026). A pipeline failure can cause environmental pollution, production loss, financial loss and regulatory penalties, and the cost of inspection, repair and remediation is magnified offshore (Amaechi et al., 2023; Du et al., 2023).

Corrosion is one of the most prevalent causes of offshore pipeline failure. Internal corrosion is associated with produced water, CO2, H2S and microorganisms in the conveyed fluid, while external corrosion is associated with coating failure, inadequate cathodic protection and the seawater environment (Melchers &

Tan, 2023; Mouneir & El-Shamy, 2026; Wasim & Djukic, 2022). Concern is growing because many offshore pipelines have been in service for decades and are approaching or exceeding their design life (Wasim & Djukic, 2022). Pipeline failures have been reported in the main African production regions, particularly the Gulf of Guinea and the Niger Delta (Amaechi et al., 2023; Iyeh & Adams, 2017; Ugwunna et al., 2018).

Failure analyses of corroded pipelines have identified CO_2 corrosion, pitting, chloride-driven attack and damaged coatings as recurring causes (Chen et al., 2021; Fawzy et al., 2024; Hussein & Abdulsada, 2026; Jianbo et al., 2021; Meng et al., 2026; Song et al., 2023). Data-driven and probabilistic approaches have been used to predict corrosion rate and failure, including neural networks and reliability models applied to Niger Delta pipelines (Alfred et al., 2022; Olaye et al., 2025), and reviews of failure prediction and residual-strength assessment are available (Khan et al., 2021; Li et al., 2022; Zakikhani et al., 2020).

In the Niger Delta, ultrasonic testing of a natural gas pipeline linked failure to corrosion and weld defects (Ugwunna et al., 2018), whereas an analysis of ten years of records for Nigeria's coastal region attributed about 98% of recorded incidents to vandalism (Nwokedi & Nnadi, 2018). Other studies have addressed fatigue of cracked or pitted pipelines (Farhad et al., 2019; Jiang et al., 2025; Kakaie et al., 2023; Olamide et al., 2020; Zhang et al., 2016) and mechanical damage from excavation, anchors, falling objects and trawl gear (Hou et al., 2025; Jiang et al., 2021; Rusin et al., 2021; Tian et al., 2021; Yuan et al., 2025).

Most of this work concerns the North Sea, the Gulf of Mexico and other mature petroleum provinces, and comparatively little addresses corrosion of offshore pipelines in Africa, where environmental conditions, operating practice, infrastructure age and regulation may differ. Several established methods estimate the remaining strength of corroded pipe: ASME B31G (ASME, 2012), modified B31G (Kiefner & Vieth, 1989), PCORRC (Stephens & Leis, 2000) and DNV-RP-F101 (Det Norske Veritas, 2010). They were developed and checked against burst-test data and finite element studies (Fu & Kirkwood, 1995; Benjamin et al., 2000; Choi et al., 2003; Cosham et al., 2007; Zhu & Leis, 2012). Nonlinear finite element analysis complements these methods because it represents the defect geometry, material hardening and large deformation directly (Netto et al., 2005; Chiodo & Ruggieri, 2009; Xu & Cheng, 2012; Sormin et al., 2024).

Finite element assessment of pipeline stress and stability has also been applied to a Gulf of Guinea pipeline and checked against DNV and ASME code requirements (Ojie et al., 2026). Numerical simulation has likewise been used to evaluate the power performance of dynamic positioning systems on offshore drilling units (Ojie et al., 2026). The aim of this study is to assess a corrosion defect in an offshore oil and gas pipeline under the design conditions of an African offshore case and to discuss the result in terms of pipeline integrity management.

The objectives are to (i) evaluate the corroded pipeline numerically using ANSYS Workbench, (ii) determine the effect of internal pressure on stress, strain and deformation in the pipe wall, (iii) examine the sensitivity of hoop stress to defect dimensions, (iv) verify the model through a mesh independence study and benchmark it against published burst tests and code-based methods, and (v) justify the failure criterion and discuss its implications for offshore pipeline integrity management in Africa.

MATERIALS AND METHODS

Case study and input data

The Medgaz gas transmission pipeline linking Algeria and Spain across the Mediterranean Sea (Fig. 1) was used as the representative case. It reaches a water depth of 2,155 m, is made of API 5L X70 steel, and was designed for a 50-year life with concrete coating thicknesses of 45 mm and 80 mm. The route crosses sandy and clayey sediments between the shore approach and the outer shelf, and buckling is possible between KP-22 and KP-37 (Koto et al., 2015). Because long-term, site-specific field data are not available for this study, published design and material data were used as mean input values (Tables 1 and 2) (Arumugam et al., 2020; Koto et al., 2015).

ISSN No. 2454-6194 | DOI: 10.51584/IJRIAS |Volume XI Issue IX September 2026

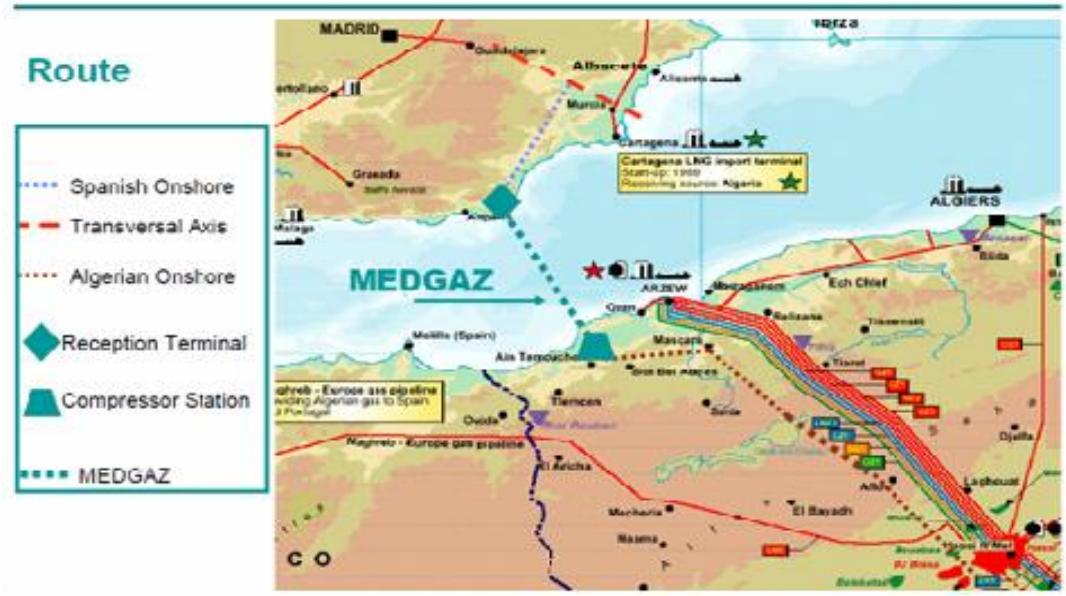


Fig. 1. Route map of the Medgaz pipeline (adapted from Koto et al., 2015).

Table 1. Pipeline design parameters.

Parameter	**Value**	**Unit**
Outside diameter	600	mm
Wall thickness	30	mm
Pipe material grade	X70	–
Thermal expansion coefficient	1.17×10^{-5}	$°C^{-1}$
Gas density	0.668	kg/m^3
Design pressure	22	MPa
Operating temperature	60	°C
Seawater density	1025	kg/m^3
Water depth	2155	m
External pressure	21.7	MPa
Ambient temperature	15	°C

Source: Koto et al. (2015). External pressure calculated as ρgh from the seawater density and water depth.

ISSN No. 2454-6194 | DOI: 10.51584/IJRIAS |Volume XI Issue IX September 2026

Table 2. Material properties of API 5L X70 steel.

Property	**Value**
Density, ρ	7850 kg/m^3
Young's modulus, E	210 GPa
Poisson's ratio, μ	0.3
Yield strength, σ_y	450 MPa
Ultimate tensile strength, σ_u	535 MPa

Source: Arumugam et al. (2020).

The material was represented with a multilinear isotropic hardening model derived from the nonlinear stress–strain behaviour of X70 steel, with large-strain and large-displacement formulations to capture the high material nonlinearity near failure.

Stress and Burst Pressure Formulations

For a pressurised straight pipe, internal pressure induces hoop, longitudinal and radial stresses. For a thin-walled cylinder the hoop stress is nearly uniform through the wall and is given by Barlow's formula, and the longitudinal stress is half the hoop stress:

$$\sigma_h = \frac{pD}{2t} \quad (1)$$

$$\sigma_L = \frac{pD}{4t} \quad (2)$$

where p is the internal pressure (MPa), D is the outside diameter (mm) and t is the wall thickness (mm). The burst pressure of a pipe with a single longitudinal corrosion defect was estimated with the allowable-stress approach of DNV-RP-F101 (Det Norske Veritas, 2010):

$$P_f = \frac{2t\sigma_u}{D - t} \times \frac{1 - d/t}{1 - (d/t)/Q} \quad (3)$$

$$Q = \sqrt{1 + 0.31\left(\frac{l}{\sqrt{Dt}}\right)^2} \quad (4)$$

where P_f is the burst pressure (MPa), d is the defect depth (mm), l is the defect length (mm) and σ_u is the ultimate tensile strength (MPa). In the numerical model, failure initiation was defined by a local stress criterion, described in Section 2.4.

Finite Element Model

The corrosion defect was idealised as rectangular, which is known to give adequate accuracy for predicting the failure pressure of corroded pipelines (Netto et al., 2005). The defect was modelled on the external surface, since internal and external defects show no significant difference in failure behaviour (Cosham et al., 2007). The defect had a depth of 20 mm (d/t = 0.667), a length of 120 mm and a length-to-width ratio of two. A symmetric quarter model was used to reduce computation time without loss of accuracy, as in earlier

ISSN No. 2454-6194 | DOI: 10.51584/IJRIAS |Volume XI Issue IX September 2026

studies of single corrosion defects (Belachew et al., 2015). The model was created in ANSYS Design Modeler with a pipe length of 1,000 mm and an additional 100 mm rigid section at one end for applying constraints (Fig. 2).

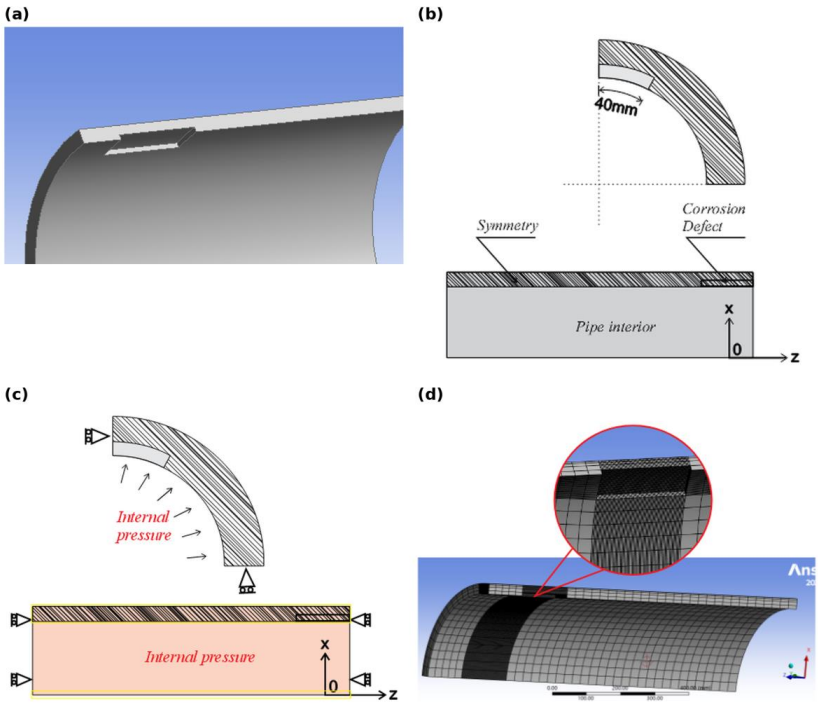


Fig. 2. (a) Three-dimensional model of the pipe with the corrosion defect; (b) symmetric quarter model; (c) quarter model showing boundary conditions and internal pressure; (d) finite element mesh at the defect.

Symmetry boundary conditions were applied on the cut faces so that the quarter model behaves as the full pipe. Rigid-body motion was prevented by restraining displacement in the x- and y-directions while allowing movement in the z-direction. Simulations were run in ANSYS Workbench 2024 (structural module). Hexahedral multi-zone meshing was used, with three element layers through the defect region, six layers elsewhere and a 3 mm element size in the defect zone (Table 3).

Table 3. Summary of mesh properties.

Property	**Value**
Mesh type	Multi-zone
General element size	30 mm
Element size in corroded zone	3 mm
Number of elements	17,860
Number of nodes	89,009

The nonlinear equilibrium equations were solved with the Newton–Raphson method, in which the displacement increment for a load increment ΔP is obtained from the tangent stiffness matrix K and the residual (out-of-balance) load vector is checked against a convergence tolerance at each iteration:

$$K(u_i)\Delta u_i = \Delta P \quad (5)$$

ISSN No. 2454-6194 | DOI: 10.51584/IJRIAS |Volume XI Issue IX September 2026

$$\Delta R_i = \Delta P - K(u_i)\Delta u_i \quad (6)$$

Internal pressure was applied incrementally to the inner surface, from 10 MPa to 45 MPa, over 500 time steps, with each load step subdivided into 100 sub-steps. The load increment was reduced automatically if the equivalent plastic strain exceeded 0.005 or if convergence was not achieved within 50 iterations, and the run was terminated if the pressure increment fell below 0.01 MPa, in which case the failure pressure was taken as the highest pressure successfully applied. Only internal gauge pressure was applied. The external hydrostatic pressure at 2,155 m (21.7 MPa, Table 1) was not applied, and all pressures in this paper, including the code-based values from Eqs. (3) and (4), are internal gauge pressures.

Failure Criterion

Failure initiation was defined as the first pressure at which the von Mises stress along a radial path through the wall at the centre of the defect reaches the ultimate tensile strength (σ_u = 535 MPa) at any point across the thickness. This criterion was adopted for three reasons. First, σ_u is the stress at which a ductile steel such as X70 can no longer carry increasing uniform load, so a local stress at σ_u marks the onset of the plastic instability that precedes burst. Second, σ_u is also the strength parameter in the DNV-RP-F101 capacity equation (Eq. 3), so the numerical and code-based pressures can be compared on the same basis. Third, the criterion can be applied directly to the ANSYS results without a damage or fracture model, which would need toughness data that are not available for this case.

Other criteria are used in pipeline burst assessment. (i) First yield of the ligament (σ_y = 450 MPa) is simple but strongly conservative for ductile pipe, because it ignores the reserve of strength between σ_y and σ_u. (ii) Flow-stress criteria relate burst to the stress averaged over the remaining ligament reaching a flow stress, taken as σ_y plus 69 MPa in modified B31G and as σ_u in PCORRC and DNV-RP-F101 (Kiefner & Vieth, 1989; Stephens & Leis, 2000); they give higher pressures than a point criterion because stress is redistributed within the ligament (Choi et al., 2003; Chiodo & Ruggieri, 2009). (iii) The average shear stress yield criterion was developed to improve burst predictions for line pipe of different grades (Zhu & Leis, 2012). (iv) True-stress and true-strain criteria declare failure when the equivalent plastic strain reaches the strain at maximum load (Xu & Cheng, 2012). (v) A global plastic-collapse criterion uses the maximum of the pressure–deformation curve. (vi) Ductile damage models, such as Gurson-type or cohesive-zone models, are needed when failure is controlled by fracture.

A point criterion based on σ_u is therefore the more conservative of the practical options. In the large-strain formulation used here ANSYS reports Cauchy (true) stress, so comparing it with the engineering value of σ_u is stricter still. Fig. 3d also shows that the maximum von Mises stress kept rising beyond 30 MPa without numerical divergence (570.0, 581.5 and 606.2 MPa at 35, 40 and 45 MPa). The value of 30 MPa is therefore the pressure at which failure initiates locally. It is a conservative lower bound on the burst pressure and not the pressure of global plastic collapse. Section 3.4.4 quantifies how sensitive the result is to this choice.

RESULTS AND DISCUSSION

Stress, strain and Deformation at Failure

Fig. 3a–c shows the total deformation, equivalent von Mises stress and equivalent elastic strain at an internal pressure of 30 MPa. The maximum total deformation was 0.54562 mm, located at the centre of the defect, where the reduced wall thickness lowers the load-bearing capacity and produces local outward bulging relative to the intact pipe. The maximum von Mises stress was 548.02 MPa, concentrated beneath the core of the defect in the circumferential direction; stress was highest at the thinnest section and decreased towards the defect edges and into the uncorroded wall. This stress exceeds the ultimate tensile strength of 535 MPa and identifies 30 MPa as the failure pressure under this criterion. The maximum equivalent elastic strain of 0.0026102 mm/mm follows the same pattern, so the failure initiation zone is the thinned material at the centre of the deep defect (d/t = 0.667).

ISSN No. 2454-6194 | DOI: 10.51584/IJRIAS |Volume XI Issue IX September 2026

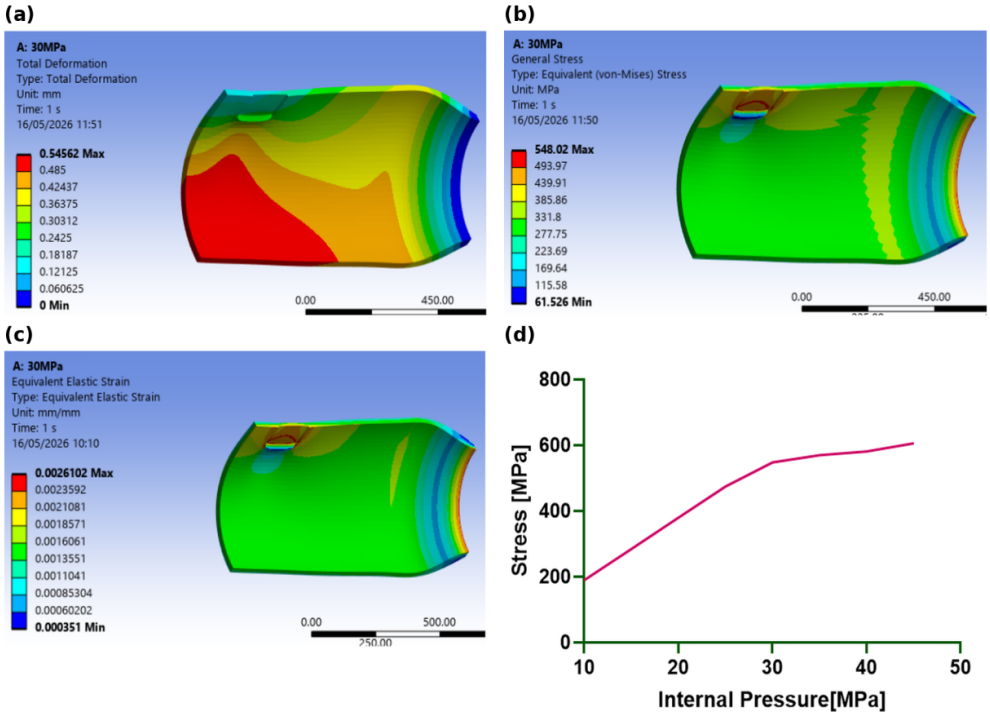


Fig. 3. Results at 30 MPa internal pressure: (a) total deformation; (b) equivalent von Mises stress; (c) equivalent elastic strain in the defect region; (d) maximum von Mises stress in the defect region as a function of internal pressure.

Effect of Internal Pressure

Fig. 3d shows the maximum von Mises stress in the defect region as internal pressure increased from 10 to 45 MPa. Between 10 and 25 MPa the stress increased almost linearly, from approximately 190 to 475 MPa. At 30 MPa it reached 548.02 MPa, above the ultimate tensile strength, which marks the failure pressure under this criterion. Beyond this point the rate of stress increase fell (570.0, 581.5 and 606.2 MPa at 35, 40 and 45 MPa), reflecting extensive plasticity and large deformation. This is the expected behaviour of a ductile pipe in which hoop stress dominates, as in pressure vessel theory, but is amplified by the local thinning at the defect. Total deformation increased steadily with pressure, from about 0.50 mm at 10 MPa to about 0.58 mm at 45 MPa (Fig. 4a), and the longitudinal stress at the defect increased from about 204 to 232 MPa (Fig. 4b). The longitudinal stress therefore remained well below the hoop stress, as theory predicts, while still contributing to the equivalent stress state. These results indicate that failure is governed mainly by hoop stress concentration in the circumferential direction at the deepest part of the defect.

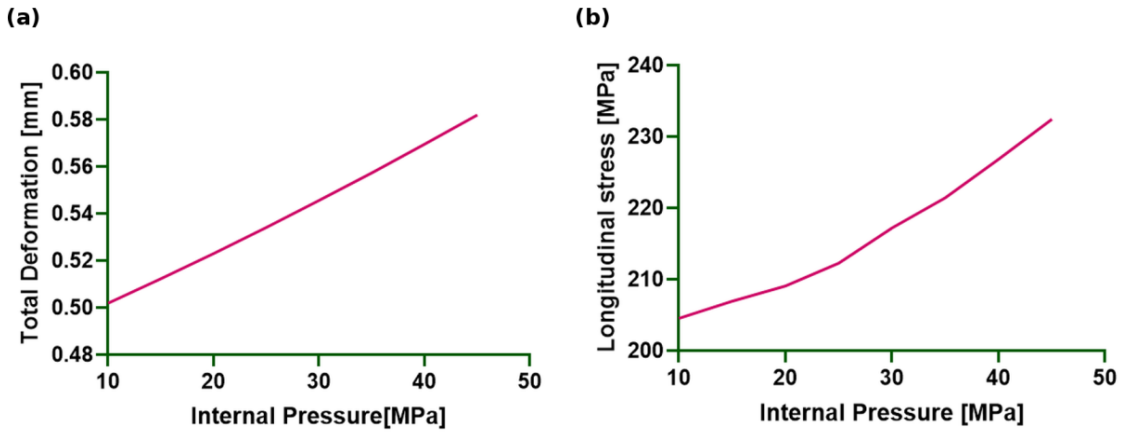


Fig. 4. Response of the defect region to internal pressure: (a) total deformation; (b) longitudinal (axial) stress.

ISSN No. 2454-6194 | DOI: 10.51584/IJRIAS |Volume XI Issue IX September 2026

Sensitivity to Defect Dimensions

The influence of defect depth, length and width on the hoop stress in the defect region was examined at the failure pressure of the baseline case, 30 MPa (Fig. 5). Hoop stress increased monotonically with defect depth, from 606.9 to 613.2 MPa over the range analysed (Fig. 5a). It decreased with increasing defect length, from 657 MPa at 60 mm to 511 MPa at 100 mm (Fig. 5b), and with increasing width, from 524 MPa at 80 mm to 503 MPa at 120 mm (Fig. 5c).

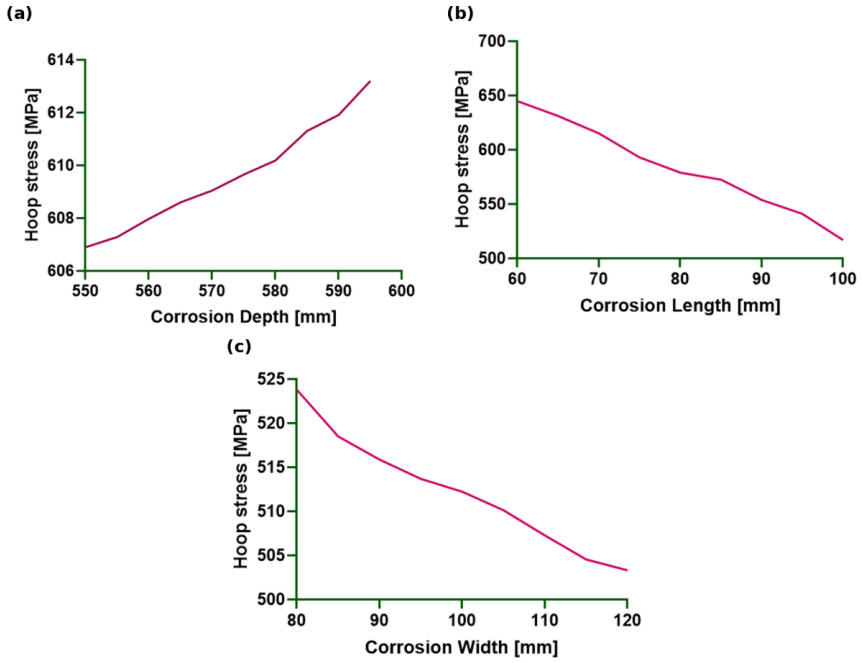


Fig. 5. Hoop stress in the defect region as a function of (a) corrosion depth, (b) corrosion length and (c) corrosion width.

Peak hoop stress and remaining strength are different quantities, and they need not change in the same direction. Peak hoop stress is a local response at a fixed pressure. It depends on how well the thinned wall is supported by the surrounding intact wall and on the stress concentration where the defect meets the full wall thickness. A likely explanation for the trends in Fig. 5b and 5c is that, as the defect is lengthened or widened at constant depth, the stress concentrations at its edges and corners move apart and the maximum on the radial

path through the centre falls. Remaining strength, by contrast, is the pressure at which the failure criterion is reached, and it depends on the load the whole thinned ligament can carry. A longer defect leaves a longer stretch of wall at reduced thickness, so the bulging region is larger and receives less support from the adjacent wall. In Eqs. (3) and (4) the factor Q increases with the length l, so the term $1 - (d/t)/Q$ decreases and P_f falls. For the baseline depth ($d/t = 0.667$), the DNV-RP-F101 failure pressure falls from 53.2 MPa at l = 60 mm to 51.1 MPa at 80 mm, 48.9 MPa at 100 mm and 46.6 MPa at 120 mm. Depth acts directly through the term $(1 - d/t)$ and through the higher stress in a thinner ligament. Eqs. (3) and (4) contain no defect width, so any effect of width on remaining strength can be resolved only by numerical analysis such as the present one.

Because the peak stresses in Fig. 5 were taken at a single pressure, they rank the geometries by local stress and not by remaining strength.

Verification, Benchmarking and Comparison With Code Methods

Mesh Independence

Mesh independence was checked by refining the defect-zone element size and the number of through-

ISSN No. 2454-6194 | DOI: 10.51584/IJRIAS |Volume XI Issue IX September 2026

thickness layers while keeping the loads, boundary conditions and failure criterion unchanged (Table 4). The response variables were the failure pressure and the maximum von Mises stress at 30 MPa, and the mesh was regarded as converged when a further refinement changed both by less than 2%.

Table 4. Mesh independence study.

Mesh	Element size in defect zone (mm)	Elements	Failure pressure (MPa)	Maximum von Mises stress at 30 MPa (MPa)	Change from previous mesh (%)
Coarse	6				–
Medium	4.5				[ ]
Baseline	3	17,860	30.0	548.02	[ ]
Fine	2				[ ]
Finer	1.5				[ ]

Comparison with Published Burst Tests

Code methods are themselves calibrated against tests, so agreement with them cannot replace comparison with measurements. The modelling procedure used here (element type, hardening curve, boundary conditions and failure criterion) was therefore applied to burst tests for which the pipe geometry, defect dimensions, material properties and measured failure pressure are reported. Candidate data sets are the small-scale burst tests of pipes with machined defects in Netto et al. (2005), the full-scale tests of pipes with long external corrosion in Benjamin et al. (2000), and the test databases reviewed by Cosham et al. (2007).

Comparison with Code-Based Methods

DNV-RP-F101 is a widely accepted recommended practice for assessing the remaining strength of corroded pipelines, calibrated with finite element analyses and full-scale burst tests (Det Norske Veritas, 2010). For a single longitudinal defect with d = 20 mm (d/t = 0.667), l = 120 mm, D = 600 mm, t = 30 mm and σ_u = 535 MPa, Eqs. (3) and (4) give Q = 1.117 and a best-estimate failure pressure of 46.55 MPa. For comparison, ASME B31G (flow stress $1.1\sigma_y$), modified B31G (flow stress σ_y + 69 MPa) and PCORRC were evaluated for the same defect (Table 5). The difference between the FEA and each method, relative to the method, is

$$\text{Difference (\%)} = \frac{P_{FEA} - P_{DNV}}{P_{DNV}} \times 100 \qquad (7)$$

Table 5. Comparison of predicted failure pressures for the baseline defect.

Method	Failure pressure (MPa)	Difference of FEA (%)	Strength parameter used
Nonlinear FEA (this study)	30.0	–	Local von Mises stress = σ_u

ISSN No. 2454-6194 | DOI: 10.51584/IJRIAS |Volume XI Issue IX September 2026

DNV-RP-F101	46.55	-35.6	σ_u = 535 MPa
PCORRC	43.12	-30.4	σ_u = 535 MPa
ASME B31G	42.12	-28.8	$1.1\sigma_y$
Modified B31G	41.86	-28.3	σ_y + 69 MPa

The FEA failure pressure is 28–36% below the code-based values, and the four code methods lie within about 11% of one another (41.9–46.6 MPa). The difference therefore comes mainly from the numerical failure criterion and not from the choice of code. The FEA value is conservative, which is consistent with a point criterion based on the engineering σ_u (Section 2.4) and with a deep defect, for which stress redistribution within the ligament is large. The design pressure of the pipeline is 22 MPa (Table 1), so the FEA failure pressure is 1.36 times the design pressure and the code-based pressures are 1.9 to 2.1 times the design pressure.

Sensitivity to the Failure Criterion

Because ANSYS reports Cauchy stress in a large-strain analysis, the engineering σ_u of 535 MPa understates the stress at which the material reaches maximum load. If the uniform strain at maximum load is ε_u, the true stress at that point is approximately $\sigma_u(1 + \varepsilon_u)$. For an assumed ε_u of 0.08 to 0.10, this gives 578 to 589 MPa. Interpolating the maximum von Mises stress in Fig. 3d (570.0 MPa at 35 MPa, 581.5 MPa at 40 MPa and 606.2 MPa at 45 MPa) places the corresponding failure pressure at about 38 to 42 MPa, close to the code-based range of 41.9–46.6 MPa. The conservatism of the 30 MPa result therefore comes largely from comparing a true stress with an engineering strength, and the value is best used as a conservative screening bound.

LIMITATIONS

The results should be read within the following limitations. First, the failure criterion is a local stress criterion based on the engineering σu, so 30 MPa is a conservative failure-initiation pressure and not the pressure of global collapse (Sections 2.4 and 3.4.4). Second, the parametric study reports hoop stress at one pressure and does not give a failure pressure for each geometry. Third, a symmetric quarter model was used, which excludes asymmetric defect shapes and weld interactions. Fourth, the study is based on published design data for a single Mediterranean pipeline and not on site-specific inspection data from the Gulf of Guinea or other African fields. Fifth, internal and external corrosion were assumed to have the same effect on the pipe section, and a single isolated defect under internal pressure only was considered, without external hydrostatic pressure (21.7 MPa at 2,155 m; Table 1), bending or axial load. External pressure reduces the net pressure on the wall, so omitting it is conservative for pressure containment, although it would matter for collapse and buckling checks.

Implications for Pipeline Integrity Management in African Operating Environments

The results support integrity management in three ways. First, they give a conservative screening bound. The deep defect (d/t = 0.667) initiates local failure at 30 MPa in the FEA and at 41.9–46.6 MPa by the code methods (Section 3.4.3), which are margins of 1.4 and 1.9–2.1 on the design pressure of 22 MPa. Such margins show how much capacity remains and when re-assessment is needed as corrosion grows. Second, the sensitivity results show that depth and length govern remaining strength, whereas peak stress at a fixed pressure is a poor ranking measure (Section 3.3). Defect sizing from in-line inspection should therefore report both depth and length, with a stated tolerance. Third, comparing code methods with FEA identifies defects that justify a more detailed assessment. Where simple methods and a conservative FEA differ by 28–36%, as here, the FEA bound can help decide whether to repair, derate or keep monitoring a defect, within a

fitness-for-service procedure such as API 579-1/ASME FFS-1 (API & ASME, 2016) and an integrity management system such as DNV-RP-F116 (DNV, 2021).

These points matter for African offshore operations for specific reasons. Many offshore pipelines are approaching or exceeding their design life (Wasim & Djukic, 2022), and failures have been reported in the Gulf of Guinea and the Niger Delta, where corrosion and weld defects have been identified as causes (Ugwunna et al., 2018) and an analysis of Nigeria's coastal region attributed most recorded incidents to vandalism (Nwokedi & Nnadi, 2018). Integrity programmes in these environments therefore need to separate corrosion-driven loss of strength from third-party damage and to direct inspection effort to the pipelines with the smallest remaining margin. Where in-line inspection data are limited or sizing accuracy is uncertain, a conservative bound such as the FEA value allows decisions without assuming that a defect is shallower than measured. The present analysis uses published data for the Medgaz pipeline, a deepwater X70 line, and not a Gulf of Guinea field case. Applying the procedure to a specific African pipeline requires its steel grade and stress–strain curve, wall thickness, operating pressure, measured defect dimensions with sizing tolerance, and corrosion rate. With these data the same workflow gives a defect-specific failure pressure and supports the choice of a re-inspection interval.

CONCLUSION

A nonlinear finite element model with material nonlinearity and large strain and displacement was used to assess a corroded API 5L X70 pipeline under internal pressure. With failure initiation defined as the von Mises stress reaching the ultimate tensile strength of 535 MPa, the failure pressure was 30 MPa, at which the maximum von Mises stress in the defect region was 548.02 MPa. Stress, strain and deformation were concentrated at the centre of the defect, and hoop stress was the dominant stress component. The parametric study showed that hoop stress at the failure pressure rose with defect depth and fell with increasing defect length and width. Because peak stress at a fixed pressure is not a measure of capacity, remaining strength has to be judged from the failure pressure, which the code methods show to decrease with defect length. The FEA pressure was 28–36% below the DNV-RP-F101, PCORRC, ASME B31G and modified B31G values (41.9–46.6 MPa). This conservatism is attributed mainly to the local criterion and to the comparison of true stress with engineering σu (Section 3.4.4), so 30 MPa is a conservative screening bound and not a prediction of global collapse. The approach provides a basis for screening corroded offshore pipelines and for prioritising re-assessment, repair or monitoring in African operating environments, subject to site-specific inspection and material data.

Future work should use full three-dimensional models to capture asymmetric defects, weld interactions and non-uniform corrosion; extend the analysis to interacting defects and combined pressure, bending and axial loads; apply probabilistic (Monte Carlo or reliability-based) treatment of defect dimensions and material properties; validate the model with laboratory burst tests on X70 specimens with machined defects; compare alternative failure criteria (true-strain, ligament-average and limit-load) on the same model; and integrate the model with real-time sensor data in a digital twin for monitoring.

ACKNOWLEDGEMENTS

The authors thank the Department of Marine Engineering, Rivers State University, Port Harcourt, and colleagues who supported this work.

Conflict of Interest

The authors declare no financial or non-financial conflicts of interest related to this work.

REFERENCES

1. Alfred, B. O., Kana, A. F., & Aliyu, S. (2022). Predicting the corrosion rate of oil and gas pipelines using neural network. Journal of Science Logics ICT Research, 8(2), 10.

2. Amaechi, C. V., Hosie, G., & Reda, A. (2023). Review on subsea pipeline integrity management: An operator's perspective. Energies, 16(1), Article 98.
3. API & ASME. (2016). Fitness-for-service (API 579-1/ASME FFS-1). American Society of Mechanical Engineers.
4. Arumugam, T., Rosli, M. K., Karuppanan, S., Ovinis, M., & Lo, M. (2020). Burst capacity analysis of pipeline with multiple longitudinally aligned interacting corrosion defects subjected to internal pressure and axial compressive stress. SN Applied Sciences, 2, Article 1201. https://doi.org/10.1007/s42452-020-2994-7
5. ASME. (2012). Manual for determining the remaining strength of corroded pipelines (ASME B31G-2012). American Society of Mechanical Engineers.
6. Belachew, C. T., Ismail, M. C., & Karuppanan, S. (2015). Strength assessment of corroded pipelines: Finite element simulations and parametric studies. International Journal of Structural Stability and Dynamics, 17, Article 1750069.
7. Benjamin, A. C., Vieira, R. D., Freire, J. L. F., & de Castro, J. T. P. (2000). Burst tests on pipeline with long external corrosion. In Proceedings of the International Pipeline Conference (IPC 2000). American Society of Mechanical Engineers.
8. Chen, B. Q., & Guedes Soares, C. (2023). Subsea pipelines. Journal of Marine Science and Engineering, 11(6), Article 1249. https://doi.org/10.3390/jmse11061249
9. Chen, Y., Wu, H., Li, J., & Chen, Y. (2021). Failure analysis of gas pipeline in a gas collecting station. Marine Science and Engineering Applications, 1(2).
10. Chiodo, M. S. G., & Ruggieri, C. (2009). Failure assessments of corroded pipelines with axial defects using stress-based criteria: Numerical studies and verification analyses. International Journal of Pressure Vessels and Piping, 86(2–3), 164–176.
11. Chohan, I. M., Ahmad, A., Sallih, N., Bheel, N., Salilew, W. M., & Almaliki, A. H. (2024). Effect of seawater salinity, pH, and temperature on external corrosion behaviour and microhardness of offshore oil and gas pipeline. Scientific Reports, 14, Article 16543.
12. Choi, J.-B., Goo, B.-K., Kim, J.-C., Kim, Y.-J., & Kim, W.-S. (2003). Development of limit load solutions for corroded gas pipelines. International Journal of Pressure Vessels and Piping, 80(2), 121–128.
13. Cosham, A., Hopkins, P., & Macdonald, K. A. (2007). Best practice for the assessment of defects in pipelines: Corrosion. Engineering Failure Analysis, 14(7), 1245–1265.
14. Deloitte. (2023). Oil and gas industry outlook.
15. Det Norske Veritas. (2010). Recommended practice DNV-RP-F101: Corroded pipelines. DNV.
16. DNV. (2021). Recommended practice DNV-RP-F116: Integrity management of submarine pipeline systems. DNV.
17. Du, F., Li, C., & Wang, W. (2023). Development of subsea pipeline buckling, corrosion and leakage monitoring. Journal of Marine Science and Engineering, 11(1), Article 188.
18. Farhad, F., Zhang, X., & Smyth-Boyle, D. (2019). Fatigue behavior of corrosion pits in X65 steel pipelines. Proceedings of the Institution of Mechanical Engineers, Part C: Journal of Mechanical Engineering Science, 233(5), 1771–1782.
19. Fawzy, J., El-Shorbagy, R. M., & Khalifa, W. (2024). Corrosion failures in oil and gas fields: Review and case studies. International Journal of Materials Technology and Innovation, 4(2), 30–38.
20. Fu, B., & Kirkwood, M. G. (1995). Predicting failure pressure of internally corroded linepipe using the finite element method. In Proceedings of the 14th International Conference on Offshore Mechanics and Arctic Engineering (Vol. 5, pp. 175–184). American Society of Mechanical Engineers.
21. Fyrileiy, O., Aamlid, O., Venas, A., & Colberg, L. (2013). Deepwater pipelines status, challenges and future trends. Journal of Pipeline Engineering, 12(3), 145–160.
22. Hou, F., Chen, Y., Yan, Y., Liu, R., Liu, Y., & Zhong, R. (2025). Structural response and damage assessment method for subsea pipe in pipe subjected to anchor impact. Marine Structures, 99, Article 103714. https://doi.org/10.1016/j.marstruc.2024.103714
23. Hussein, N. K., & Abdulsada, S. A. (2026). Analysis of internal corrosion and failure in oil pipelines from a metallurgical perspective: A brief review. Petroleum & Coal, 68(1), 168–185.
24. International Energy Agency. (2024). Global gas security review. IEA.

25. Iyeh, E., & Adams, G. (2017). Offshore pipeline failure root cause analysis [Paper presentation]. Abu Dhabi International Petroleum Exhibition and Conference (ADIPEC), Abu Dhabi, United Arab Emirates. Society of Petroleum Engineers.
26. Jianbo, J., Liang, D., & Tao, M. (2021). Failure analysis on leakage and perforation of natural gas pipeline. Journal of Physics: Conference Series, 1885, Article 022026. https://doi.org/10.1088/1742-6596/1885/2/022026
27. Jiang, D., Huang, X., Zhao, D., Yang, H., & Tang, G. (2025). Fatigue life prediction of submarine pipelines with varying span length and position. Journal of Marine Science and Engineering, 13(4), Article 763. https://doi.org/10.3390/jmse13040763
28. Jiang, F., Dong, S., & Li, X. (2021). Risk based integrity model for offshore pipelines subjected to impact loads from falling object. Proceedings of the Institution of Mechanical Engineers, Part M: Journal of Engineering for the Maritime Environment, 235(2), 385–400. https://doi.org/10.1177/1475090220960562
29. Kakaie, A., Guedes Soares, C., Ariffin, A. K., & Punurai, W. (2023). Fatigue reliability analysis of submarine pipelines using the Bayesian approach. Journal of Marine Science and Engineering, 11(3), Article 580. https://doi.org/10.3390/jmse11030580
30. Khan, F., Rathnayaka, S., & Ahmed, S. (2021). Risk-based pipeline integrity management: A road map to resilient pipelines. Journal of Pipeline Science and Engineering, 1(1), 74–87. https://doi.org/10.1016/j.jpse.2021.02.001
31. Kiefner, J. F., & Vieth, P. H. (1989). A modified criterion for evaluating the remaining strength of corroded pipe (Report PR 3-805). Pipeline Research Committee, American Gas Association.
32. Koto, J., Abdul, K. J., & Selemat, A. (2015). Ultra deep water subsea pipeline design and assessment. Science and Engineering, 2.
33. Li, H., Huang, K., Zeng, Q., & Sun, C. (2022). Residual strength assessment and residual life prediction of corroded pipelines: A decade review. Energies, 15(3), Article 726.
34. Melchers, R. E., & Tan, M. Y. (2023). Long-term corrosion of abandoned offshore steel infrastructure. Corrosion Engineering, Science and Technology, 58(8).
35. Meng, Q., Yan, Y., Wu, J., Zhou, J., Li, Y., Li, J., & Ren, J. (2026). Failure analysis of a single crude oil pipeline rupture at an oilfield in western China. Journal of Physics: Conference Series, 3202, 012044. https://doi.org/10.1088/1742-6596/3202/1/012044
36. Monde, L. (2024). New African frontier for offshore oil development.
37. Mouneir, S. M., & El-Shamy, A. M. (2026). A comprehensive review of corrosion in oil and gas pipelines: Mechanisms, mitigation strategies, and future directions. Multiscale and Multidisciplinary Modeling, Experiments and Design, Article 131.
38. Netto, T. A., Ferraz, U. S., & Estefen, S. F. (2005). The effect of corrosion defects on the burst pressure of pipelines. Journal of Constructional Steel Research, 61(8), 1185–1204.
39. Nwokedi, T. C., & Nnadi, K. U. (2018). Estimating the theoretical and empirical probability coefficient of oil pipeline transport infrastructure failure modes in Nigeria's coastal ecosystem: Panacea for non optimal deployment of pipeline safety and security management systems. Scientific Journal of Transport and Logistics, 9(2).
40. Ojie, E. E., Inegiyemiema, M., & Nitonye, S. (2026a). Offshore pipeline stress and stability analysis in the Gulf of Guinea. International Journal of Research and Innovation in Applied Science. https://doi.org/10.51584/IJRIAS.2026.11080065
41. Ojie, E. E., Nwoka, B. G., & Ekine, A. A. (2026b). Adaptive thruster allocation and integrated performance evaluation for dynamic positioning of semisubmersible drilling units. Global Journal of Engineering and Technology Advances, 28(3), 298–311. https://doi.org/10.30574/gjeta.2026.28.3.0264
42. Olamide, A., Bennecer, A., & Kaczmarczyk, S. (2020). Finite element analysis of fatigue in offshore pipelines with internal and external circumferential cracks. Applied Mechanics, 1(4), 193–223.
43. Olaye, M., Akinfaloye, A., & Amadhe, F. (2025). Investigation of pipeline failure and corrosion rate prediction using a reliability model for pipeline integrity and safety. Saudi Journal of Engineering and Technology, 10(11), 576–582.
44. Rusin, A., Stolecka-Antczak, K., Kapusta, K., Rogozinski, K., & Rusin, K. (2021). Analysis of the effect of failure of a gas pipeline caused by mechanical damage. Energies, 14(22), Article 7686.

https://doi.org/10.3390/en14227686

45. Song, C., Li, Y., Wu, F., Luo, J., Li, L., & Li, G. (2023). Failure analysis of the crack and leakage of a crude oil pipeline under CO_2-steam flooding. Processes, 11(5), Article 1567. https://doi.org/10.3390/pr11051567
46. Sormin, M. Y., Hadiwidodo, Y. S., & Syahroni, N. (2024). Burst pressure analysis on corroded pipeline using finite element method. International Journal of Offshore and Coastal Engineering, 8(2), 108–116.
47. Stephens, D. R., & Leis, B. N. (2000). Development of an alternative failure criterion for residual strength of corrosion defects in moderate- to high-toughness pipe. In Proceedings of the International Pipeline Conference (IPC 2000) (Vol. 2, pp. 781–792). American Society of Mechanical Engineers.
48. Tian, Y., Borgi, S. E., Zhang, C., Sun, L., Xiao, Z., & Fu, D. (2021). Assessment of submarine pipeline damages subjecting to falling object impact considering the effect of seabed. Marine Structures, 78, Article 102963. https://doi.org/10.1016/j.marstruc.2021.102963
49. Ugwunna, A. D., Appah, D., & Evbuomwan, B. O. (2018). Analysis of natural gas pipeline failure (a case study of a typical marginal oil and gas field in the Niger Delta, Nigeria). Saudi Journal of Engineering and Technology, 3(12), 672–679.
50. Wasim, M., & Djukic, M. B. (2022). External corrosion of oil and gas pipelines: A review of failure mechanism and preventions. Journal of Natural Gas Science and Engineering, 100, Article 104467. https://doi.org/10.1016/j.jngse.2022.104467
51. Xu, L. Y., & Cheng, Y. F. (2012). Reliability and failure pressure prediction of various grades of pipeline steel in the presence of corrosion defects and pre-strain. International Journal of Pressure Vessels and Piping, 89, 75–84.
52. Yan, J., Zhang, Y., & Chen, Z. (2026). Pipeline systems in floating offshore production systems: Hydrodynamics, corrosion, design and maintenance. Journal of Marine Science and Engineering, 14(2), Article 176. https://doi.org/10.3390/jmse14020176
53. Yuan, Z., Zou, H., & Azimi, M. (2025). Characteristics of trawling forces on submarine pipelines by fishing vessel trawl gear. Urban Lifelines. https://doi.org/10.1007/s44285-025-00056-1
54. Zakikhani, K., Nasiri, F., & Zayed, T. (2020). A review on failure prediction models for oil and gas pipelines. Journal of Pipeline Systems Engineering and Practice, 11(1), Article 03119001.
55. Zhang, Y., Fan, M., Xiao, Z. M., & Zhang, W. G. (2016). Fatigue analysis on offshore pipelines with embedded cracks. Ocean Engineering, 117, 45–56.
56. Zhu, H., Chen, J., Lin, Y., Guo, J., Gao, X., Chen, Y., Ge, Y., & Wang, W. (2024). In-line inspection (ILI) techniques for subsea pipelines: State-of-the-art. Journal of Marine Science and Engineering, 12(3), Article 417. https://doi.org/10.3390/jmse12030417
57. Zhu, X.-K., & Leis, B. N. (2012). Evaluation of burst pressure prediction models for line pipes. International Journal of Pressure Vessels and Piping, 89, 85–97.